ORIGINAL ARTICLE

Temporal Registration of Cardiac Multimodal Images Using Locally Linear Embedding Algorithm

Talayeh Ghodsizad [1], Hamid Behnam [2*], Emad Fatemizadeh [3], Taraneh Faghihi Langroudi [4], Fariba Bayat [5]

[1] *Department of Biomedical Engineering, Science and Research Branch, Islamic Azad University, Tehran, Iran*

[2] *Department of Biomedical Engineering, Iran University of Science and Technology, Tehran, Iran*

[3] *School of Electrical Engineering, Sharif University of Technology, Tehran, Iran*

[4] *Department of Radiology, Modarres Hospital, Shahid Beheshti University of Medical Sciences, Tehran, Iran*

[5] *Cardiovascular Research Center, Modarres Hospital, Shahid Beheshti University of Medical Sciences, Tehran, Iran*

*Corresponding Author: Hamid Behnam
Email: behnam@iust.ac.ir

Received: 19 June 2021 / Accepted: 06 August 2021

Abstract

Purpose: Multimodal Cardiac Image (MCI) registration is one of the evolving fields in the diagnostic methods of Cardiovascular Diseases (CVDs). Since the heart has nonlinear and dynamic behavior, Temporal Registration (TR) is the fundamental step for the spatial registration and fusion of MCIs to integrate the heart's anatomical and functional information into a single and more informative display. Therefore, in this study, a TR framework is proposed to align MCIs in the same cardiac phase.

Materials and Methods: A manifold learning-based method is proposed for the TR of MCIs. The Euclidean distance among consecutive samples lying on the Locally Linear Embedding (LLE) of MCIs is computed. By considering cardiac volume pattern concepts from distance plots of LLEs, six cardiac phases (end-diastole, rapid-ejection, end-systole, rapid-filling, reduced-filling, and atrial-contraction) are temporally registered.

Results: The validation of the proposed method proceeds by collecting the data of Computed Tomography Coronary Angiography (CTCA) and Transthoracic Echocardiography (TTE) from ten patients in four acquisition views. The Correlation Coefficient (CC) between the frame number resulted from the proposed method and manually selected by an expert is analyzed. Results show that the average CC between two resulted frame numbers is about 0.82±0.08 for six cardiac phases. Moreover, the maximum Mean Absolute Error (MAE) value of two slice extraction methods is about 0.17 for four acquisition views.

Conclusion: By extracting the intrinsic parameters of MCIs, and finding the relationship among them in a lower-dimensional space, a fast, fully automatic, and user-independent framework for TR of MCIs is presented. The proposed method is more accurate compared to Electrocardiogram (ECG) signal labeling or time-series processing methods which can be helpful in different MCI fusion methods.

Keywords: Multimodal Temporal Registration; Manifold Learning Algorithm; Locally Linear Embedding; Nonlinear Dimension Reduction.

DOI: https://doi.org/10.18502/fbt.v8i4.7757

1. Introduction

According to World Health Organization (WHO) statistics, CVDs are the first cause of death worldwide [1]. Early detection of CVDs leads to more effective treatment in a shorter time. Nowadays, medical imaging plays an essential role in the early diagnosis of CVDs, thus reducing mortality rates [2]. In clinically routine, physicians may request for one or more imaging modalities to produce complementary information of anatomical and functional behavior of the heart to diagnose the CVDs. Recently, the advancements in multimodal medical image registration and fusion techniques gatherers complementary information of different modalities into a single spatio-temporal reference instead of comparison in a side-by-side manner [3, 4].

The heart is a dynamic organ that changes in volume, and the heart's deformation occurs during the cardiac cycle. Important information can be extracted from the function of the heart in cardiac cycles [5]. Furthermore, TR in MCI registration is the first and essential issue to ensure that images are in the same cardiac phase. Several papers proposed MCI registration methods [6-10]. Multiple studies used ECG signals for time-stamping and TR of MCIs which depends on the level of the user's skill. [11] presents a method for the fusion of aortic valve in 2D echocardiography and CTCA as intra-procedural guidance. They used ECG time-stamping method to find the temporal correspondence between two modalities. To eliminate radiation exposure in operating rooms, [12] presented a navigation system by registering the intraoperative ultrasound and preoperative Computed Tomography (CT) images using a magnetic tracking system. In their proposed method, the preoperative CT volume is synchronized with the real-time ultrasound imaging using ECG signals in the operating room. Several studies used only one cardiac phase for MCI registration which does not consider the heart's dynamic nature. [13] presents a framework for the registration of 3D+t cine-Magnetic Resonance Imaging (MRI) and a single phase of CT scan. CT scan data are reconstructed in 75% of the cardiac cycle in Parasternal Short-Axis (PSAX) view and co-registered with the left chambers segmented from MRI images. In [14], a framework for the fusion of CTCA and MRI is proposed. They aim to quantify the relationship between coronary artery stenosis and heart perfusion imperfections. The coronary arteries are segmented from CTCA data in the diastolic phase, while Cardiac MR perfusion data are acquired in a systolic phase; thus, several inappropriate registration results in the apex of the Left Ventricle (LV) are observed in their study. [15] presented a CTCA to MRI registration framework based on the myocardial surfaces. They used the recorded ECG signal during CTCA acquisition to identify the closest MRI temporal phase to the center of the CTCA reconstruction window. A couple of studies proposed Dynamic Time Warping (DTW) methods to synchronize MCIs which need pre-processing on images to produce time series as the algorithm's inputs. [16] proposed a method for spatio-temporal registration of dynamic CT and cine-MRI. Normalized Cross-Correlation (NCC) curves of both modalities were aligned using an adapted DTW method. Another research [17] used NCC curves and their derivatives as the DTW inputs for TR of 3D echocardiography and cardiac MRI in four cardiac phases. In [18], Fourier decomposition of contours resulting from Speckle Tracking Echocardiography (STE) is used for the DTW algorithm. Their proposed method was used to spatiotemporally register CTCA and STE to achieve the optimal pacing in the cardiac resynchronization therapy. Their proposed method needs contours of cardiac chambers resulted from the STE or border extraction methods which are exhaustive due to the multiplicative speckle noise.

As the significant impact of medical image processing in the diagnosis and treatment planning of CVDs, the amount of data is continuously increasing via medical imaging technologies. Each data itself is highly complex and requires lots of storage space and time to be processed [19]. The common TR method based on ECG signal labeling depends on the user's skill as well as spending time. Although this signal is available for some recorded data such as TTE, it is not available for CTCA images in offline processing. Some algorithms, such as DTW, also require preprocessing of two modalities involved in the registration and ultimately fusion to produce time series. TR of MCIs methods has limitations. Moreover, some other studies considered registration or fusion only in one cardiac phase. In this paper, to consider these issues and investigate changes in the anatomical and functional characteristics of heart during the cardiac cycle, an entirely automatic and fast method based on dimension reduction of data is presented. The proposed method aims to synchronize functional and anatomical MCIs using LLE method. LLE is a nonlinear unsupervised dimensionality reduction method [20, 21]. It represents a low-dimensional parameterization of data sets that lie on nonlinear manifolds in high-dimensional space; consequently, the relationship among images in a low-

dimensional space will be expressed. In MCIs, instead of the apparent dimension of images, which is the size of the image, the images related to one patient may vary in a small number of parameters (e.g., noise, motions caused by heartbeat, and imaging geometry) [22]. In the proposed method, using LLE to MCIs, the structure within and among modalities is achieved. According to LLE features, similar images in the high-dimensional space will be neighbors in the lower-dimensional space. As a result, by calculating the Euclidean distance among points on the manifold, helpful information is obtained from the relationship among images in the time dimension. The proposed method is evaluated on TTE data as the functional, and CTCA as the anatomical modality recorded by our team from ten patients in four acquisition views.

This paper continues as follows: TR of TTE and CTCA images are explained in section 2. The experimental results are presented in section 3. Section 4 discusses the proposed method and the results, and finally, conclusions and perspectives of this research are described in section 5.

2. Materials and Methods

This study aims to register MCIs in six cardiac phases temporally. The framework of the study is depicted in Figure 1.

2.1. Data Collection

According to Helsinki Declaration, with the study's approval by Regional Committee for Medical research ethics, TTE, and CTCA data of ten patients who were scheduled to undergo CTCA were acquired by our team from July till November, 2017. Eight of the enrolled patients were given Metoprolol (50-100mg) due to the high heart rate. According to the ethical and legal requirements for research involving human participants [23], all cases were given written informed consent. Furthermore, a form that was duly explained by the researcher and attested by a signature of the patient was obtained from each subject [24]. The demographic data of enrolled patients are indicated in Table 1.

Table 1. Demographic data of enrolled patients (n=10)

Age	61±10 years
Male/Female	6/4
Dyspnea	10/10 (100%)
Chest pain	10/10 (100%)
Coronary Artery Bypass Grafting	3/10 (30%)
Hypertension	7/10 (70%)
Diabetes Mellitus	2/10 (20%)

CTCA: CTCA data, as the anatomical reference, were acquired with a multi-slice CT scanner (Brilliance 64; Philips Medical System, Cleveland, OH). CTCA volumes were reconstructed every 10% of the RR-interval by retrospective ECG-gating (Figure 2). Thus, the CTCA data for each patient has nine 3D volumes consisting of 368 to 465 slices of 512 × 512 pixels and slice thickness of 0.63mm.

TTE: An expert cardiologist acquired standard Apical four- Chamber (A4C), Apical two- Chamber (A2C), Parasternal Long-Axis (PLAX), and PSAX views of each patient on the same day of CTCA scanning. To evaluate the proposed algorithm for different image qualities, TTE was performed using two echocardiography systems, IE33 (Philips medical system, USA), and Vivid7 (General Electric, Horten, Norway) ultrasound systems.

The images have 800 × 600 and 636 × 420 pixels, respectively. The acquisition frame rate was 60–80 frame/second and covering 3-4 consecutive cardiac cycles, starting from the R wave. Patient heart rates during TTE acquisition ranged from 50 to 78 beats per minute.

2.2. Manifold Learning Algorithm (MLA)

Due to the increasing advancement of technology, processing systems are faced with large datasets which may contain redundant information. Feature extraction methods are used to extract intrinsic properties of the data which can express the characteristics of data in a more informative lower-dimension space [25]. MLAs are nonlinear dimensionality reduction approaches. In these methods, while maintaining the original structure

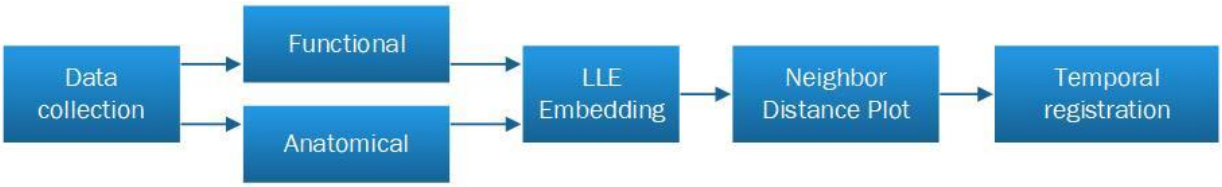

Figure 1. The flowchart of the study

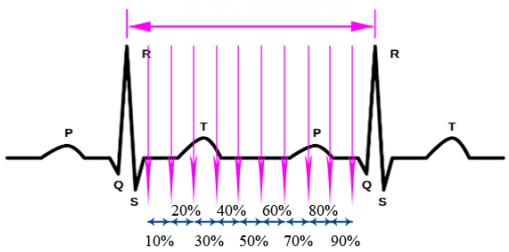

Figure 2. Schematic of retrospective ECG-gating reconstruction of CTCA data in every 10% of the RR-interval

of features, the correlated features which are the principal factor in discriminating the data from each other are combined [19]. Then, the whole dataset is placed on a manifold that expresses the actual relationship of the parameters. In other words, each data point is a sample of a smooth low-dimensional manifold embedding in a high-dimensional space [22].

Based on the nonlinear changes of heart dynamics during the cardiac cycle, linear dimension reduction methods are not responding to MCI processing. Recently, MLAs have begun to be applied to medical image analysis. MLA methods are assumed that in each N×N image, each pixel represents a dimension. Hence the apparent dimension of the image is N^2 which can be a very large number. According to the slight differences among frames of each of the two modalities, instead of an apparent dimension of each image set, there should be a new representation in a lower-dimensional space using MLAs [22].

2.3. LLE Algorithm

LLE algorithm, introduced by [26], is a nonlinear unsupervised dimension reduction method which preserves preserves the local structure of data [19]. In this method, the local property of manifold data is reconstructed by the nearest neighbors' linear composition, and a set of coefficients is obtained [19]. Then, in dimension reduction, an attempt is made to maintain these coefficients in the reconstruction [27]. This algorithm is implemented without measuring the distance or the relationship among distant points. For a data set called $X = \{x_i\}, i = 1 \dots N$, the LLE aims to (Equation 1):

$$x_1, x_2, \dots, x_n \in R^D \xrightarrow{f} y_1, y_2, \dots, y_n \in R^d, d \ll D \quad (1)$$

Where f is a mapping function to reconstruct X in D dimensional space to a new data set $Y = \{y_i\}, i = 1 \dots N$ in d dimensional space. LLE algorithm is summarized as follows:

1- K-nearest neighbor of each data on data set X is calculated using Euclidean distance.

2- For each connected pair of nodes (x_i, x_j), compute weights w_{ij} by minimizing $E(W)$ function (Equation 2):

$$E(W) = \sum_{i=1}^{N} \left\| \vec{x}_i - \sum_{j=1}^{k} w_{ij} \vec{x}_j \right\|^2 \quad (2)$$

Subject to $\sum_{j=1}^{k} w_{ij} = 1$

Such that $w_{ij} = 0$ if x_i and x_j are not neighbors. By considering a specific data x with its k nearest neighbors $\vec{\eta}_j$ and reconstruction weights w_j, Equation 2 can be rewritten as Equation 3:

$$\varepsilon = \left|\vec{x} - \sum_j w_j \vec{\eta}_j\right|^2 = \left|\sum_j w_j \vec{x} - \sum_j w_j \vec{\eta}_j\right|^2 = \left|\sum_j w_j (\vec{x} - \vec{\eta}_j)\right|^2, with\ |z|^2 = z^T.z = \underbrace{\left[\sum_j w_j (\vec{x} - \vec{\eta}_j)\right]^T}_{=z^T} . \underbrace{\left[\sum_k w_k (\vec{x} - \vec{\eta}_k)\right]}_{=z} = \sum_j w_j (\vec{x} - \vec{\eta}_j)^T . \sum_k w_k (\vec{x} - \vec{\eta}_k) = \sum_j \sum_k w_j \left(\vec{x} - \vec{\eta}_j\right) . w_k (\vec{x} - \vec{\eta}_k) = \sum_j \sum_k w_j\, w_k (\vec{x} - \vec{\eta}_j) . (\vec{x} - \vec{\eta}_k) = \sum_{jk} w_j w_k G_{jk} \quad (3)$$

G_{jk} is called the Gram matrix which is symmetric and semipositive definite (Equation 4),

$$G_{jk} = (\vec{x} - \vec{\eta}_j) . (\vec{x} - \vec{\eta}_k) \quad (4)$$

Using a Lagrange multiplier to enforce the $\sum_j w_j = 1$ constraint, the reconstruction error can be minimized. The optimal weights are given by Equation 5:

$$w_j = \frac{\sum_{k=1}^{K} G_{jk}^{-1}}{\sum_{l=1}^{K} \sum_{m=1}^{K} G_{lm}^{-1}} \quad (5)$$

In cases where the matrix is singular or nearly singular, it should be regularized by Equation 6:

$$\begin{cases} G_{jk} \leftarrow G_{jk} + \delta_{jk} \left(\frac{\Delta^2}{K}\right) Tr(G) & \\ \delta_{jk} = 1 & \text{if } j = k \\ \delta_{jk} = 0 & \text{otherwise} \end{cases} \quad (6)$$

Where $Tr(G)$ is the trace of the Gram matrix and $\Delta^2 \ll 1$ [27].

3- Finally, x_i in D dimensional space is mapped to y_i in d dimensional space. Because data are on or near a d dimensional manifold, a linear function consisting of translation, rotation, and scaling is considered that maps high-dimensional space to the intrinsic dimensional manifold. In this mapping, the w_{ij} coefficients are designed so that the geometric properties of the data to these linear transformations remain constant. Hence, the reconstruction coefficients in D should reconstruct the data in the d

dimensional space by minimizing the following function with respect to y_i (Equation 7):

$$\varphi(y) = \sum_{i=1}^{N} \left| \vec{y}_i - \sum_{j=1}^{k} w_{ij} \vec{y}_j \right|^2 \quad (7)$$

This function, as the function in (2) tries to minimize the reconstruction error with the difference that, in (2), y_i's are reconstructed only by w_{ij} coefficients. The dimensionality reduction is made by preserving the geometric information obtained from the coefficients. For solving this problem, Eigen value-vector analysis is used:

$$\varphi(Y) = \sum_i \left| \vec{Y}_i - \sum_j w_{ij} \vec{Y}_j \right|^2 = \sum (\vec{Y}_i - \sum_j w_{ij} \vec{Y}_j)(\vec{Y}_j - \sum_i w_{ij} \vec{Y}_i) = \sum_{ij} M_{ij} (\vec{Y}_i \vec{Y}_j) \quad (8)$$

Where $M_{ij} = \delta_{ij} - w_{ij} - w_{ij} + \sum_k w_{ki} w_{kj}$. The embedding **Y** is then given by the eigenvectors $u_0, \dots, u_d$ of M with associated eigenvalues $(\lambda_0 \leq \cdots \leq \lambda_d)$ [26, 28].

2.4. LLE in MCI Processing

The cardiac cycle consists of seven phases. The characteristics of each phase are tabulated in Table 2 [29]. As presented in Table 2, since all valves are closed during isovolumetric contraction and relaxation phases, there are no noticeable changes in the cardiac volume. Moreover, in the reduced filling phase, due to the small amount of blood entering the ventricles, there are small changes in the volume of the ventricles. Thus, in a cardiac cycle, there are three phases (second, fifth, and seventh) in which the volume of the ventricles is almost nearly constant. As a result, the MCIs of the frames associated with these phases are very similar. Besides, there are three phases (first, third, and sixth) where volume change occurs significantly. It is expected that by dimension reduction of MCIs using the LLE algorithm, the frames corresponding to the second, fifth, and seventh cardiac phases stay close to their neighboring images. The distance among the frames corresponding to the first, third, and sixth cardiac phases and their neighbors is more than other cardiac phases when mapping from high-dimensional to low-dimensional space.

3. Results

The proposed method is applied to ten collected TTE and CTCA data. Each frame of each TTE is a grayscale image of 800 × 600 and 636 × 420 pixels, so each frame's apparent dimensions (D) are 480000 and 267120, respectively. Moreover, each frame of each CTCA set is a grayscale image of 512 × 512 pixels, so the apparent dimension of each frame (D) is 262144. Although the apparent dimension of each TTE and CTCA image set is a large number, they differ in a limited number of parameters (deformation and alternating volume of the heart due to heart rate) that the LLE algorithm can extract. Figure 3 shows the LLE embedding of TTE and CTCA images in a cardiac cycle for A4C, A2C, PSAX, and PLAX cardiac views. A set of the images of four cardiac acquisition views in a cardiac cycle of TTE and CTCA are embedded in two-dimensional space using the LLE algorithm. As shown in Figure 3, due to the different structure and nonlinear dynamics of the heart, similar manifolds are not obtained in different views of the two modalities.

Table 2. Description of seven phases of the cardiac cycle

Cardiac phase		Description
Number	**Name**	
1	Atrial Contraction	- Depolarization of the atria - The blood inside the atria is pumped out into the ventricles
2	Isovolumetric Contraction	-Starts with: Closure of the mitral and tricuspid valves -Ends with: Opening of the aortic and pulmonary valves -The ventricular pressure suddenly increases due to its contraction without any changes in its volume
3	Rapid Ejection	Rapid and primary drainage of blood (70%) to the aortic, and pulmonary arteries from the left and right ventricles
4	Reduced Ejection	The rest of the blood (30%) in ventricles discharges
5	Isovolumetric Relaxation	-Starts with: Closure of the aortic and pulmonary valves -Ends with: Opening of the mitral and tricuspid valves -The ventricular pressure decreases without any changes in its volume
6	Rapid Filling	The rapid flow of the blood from the atria to the ventricles
7	Reduced Filling	-Ventricles are at the end of the filling phase -No noticeable changes in the volume of the ventricles occur

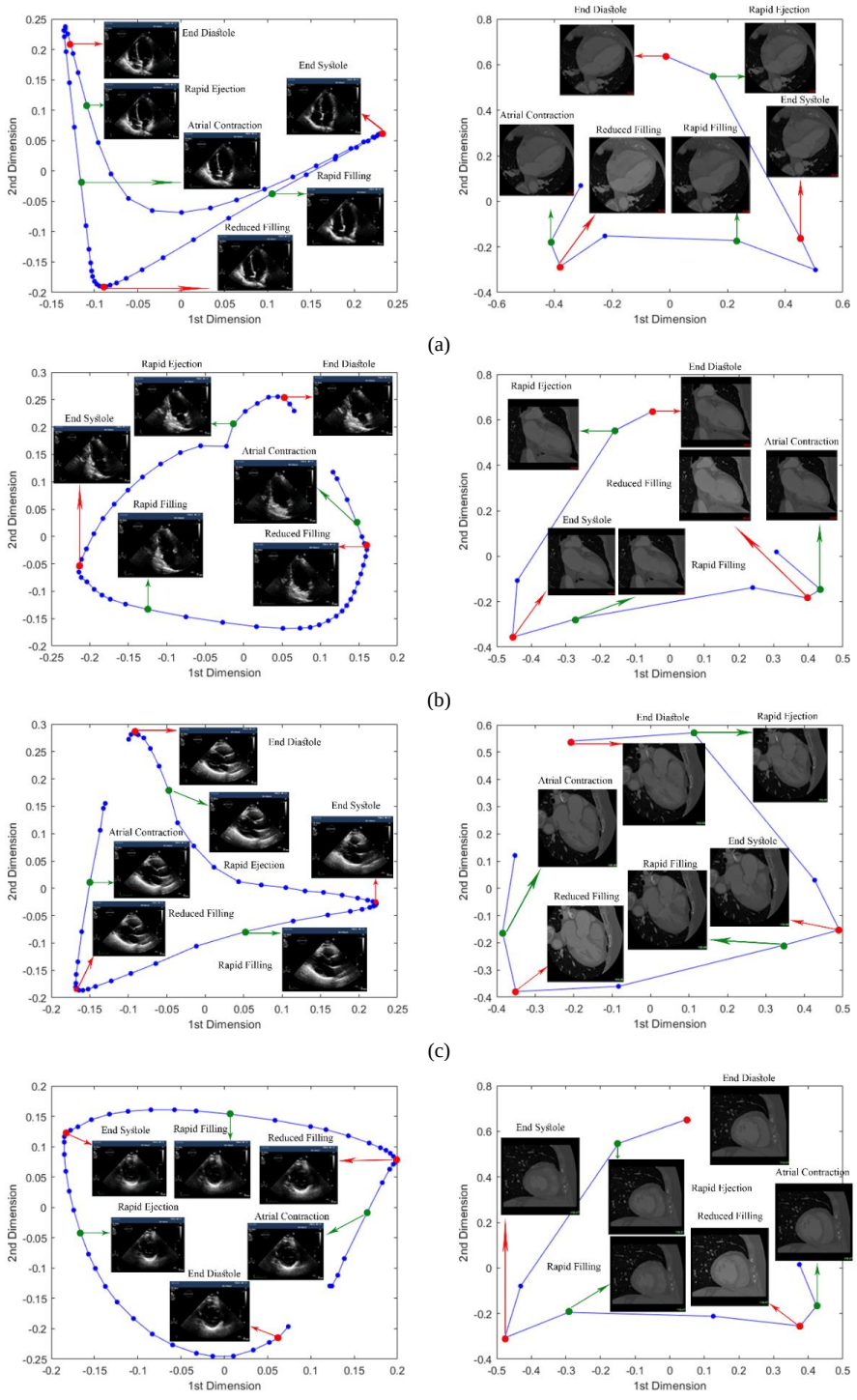

Figure 3. LLE embedding of TTE frames (left column) and CTCA slices (right column) in a cardiac cycle for a) A4C, b) A2C, c) PLAX, and d) PSAX views. Red points and arrows indicate the isovolumetric cardiac phases. The green points and arrows correspond to rapid ventricular volume change between each of the isovolumetric cardiac phases

Regarding the periodic nature of the heart's motion, all resulted manifolds are nearly closed curves. Moreover, there are no perceptible volume changes in the cardiac cycle in three end-diastole, rapid-ejection, and end-systole cardiac phased. Thus, there are three regions with a high density of points on each manifold which means they are similar in the first space (D). Due to the rapid filling of ventricles between end-systole and reduced-filling and the rapid ejection of them between end-systole and end-diastole, a dominant ventricular volume change occurs, resulting in three sparser regions on manifolds. According to the results of applying the LLE method to both modalities' image sets, six areas with prominent features are achieved. To quantify the resulted manifolds, the Euclidean distance among consecutive points on the manifolds (called the Neighbor Distance Plot (NDP) in this paper) is calculated. Figure 4 shows NDPs of LLE embedding of TTE and CTCA images. As resulted, in NDP of both modalities, three points with the

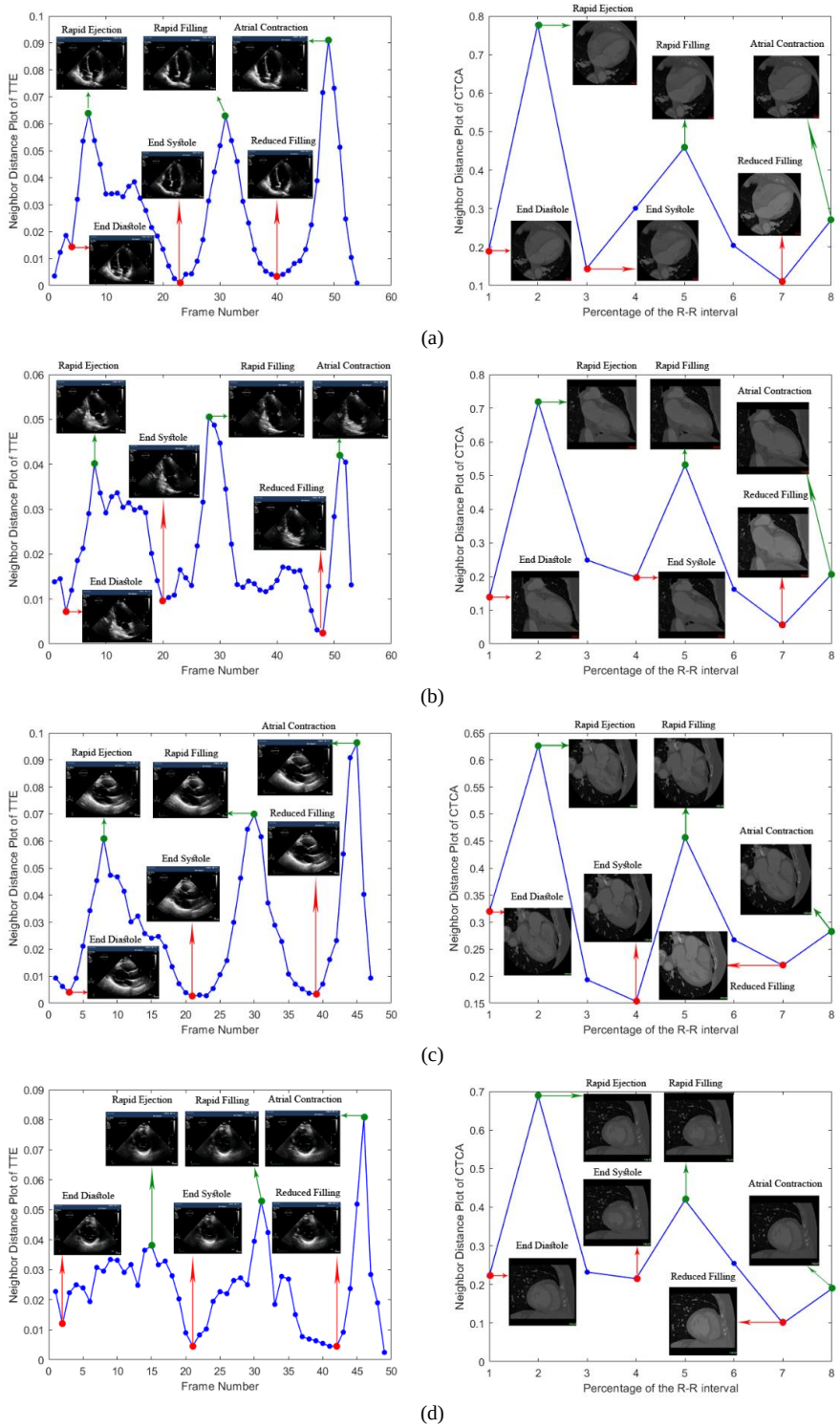

Figure 4. NDP of LLE embedding in Figure 3 for TTE frames (left column) and CTCA slices (right column) in a cardiac cycle for a) A4C, b) A2C, c) PLAX, and d) PSAX views. Red points and arrows indicate the isovolumetric cardiac phases. The green points and arrows correspond to rapid ventricular volume change between each of the isovolumetric cardiac phases

shortest distance and three points with the most considerable distances are identified. An important issue to determine landmarks on the NDP of TTE sets is that, since TTE data are started from the R wave and in contrast, the NDP of CTCA starts from the 10% of RR interval, the first and the last points of TTE's NDP are not considered as the target landmarks. As expected and depicted in Figure 4, due to the presence of three dense regions on the manifolds, whose distances are very close, three minima are observed in the NDPs corresponding to end-diastole, rapid-ejection, and end-systole cardiac phases. Also, because of the considerable volume changes in the rapid-ejection, rapid-filling, and atrial-contraction cardiac phases, three sparser regions are leading to three maxima on the NDPs. Thus, in both TTE and CTCA modalities, six cardiac phases are extracted and temporally aligned.

The evaluation of the proposed method has proceeded in two steps. First, the Correlation Coefficient (CC) among manual frame selections by an expert cardiologist as the Ground Truth (GT) and resulting frames from the proposed method. Suppose that X and Y are sets of frame numbers of GT and from the proposed method, with the mean values of μ_X and μ_Y, respectively, then, the CC is calculated as:

$$Corr(X,Y) = \frac{\mathbb{E}[(X-\mu_X)(Y-\mu_Y)]}{\sigma_X \sigma_Y} \quad (9)$$

Where σ_X and σ_Y are the standard deviations of X and Y, respectively, and $\mathbb{E}$ is the mathematical expectation. Second, to investigate the effect of selected slice from CTCA volume in the proposed method, the Mean Absolute Error (MAE) among resulting frames from the proposed method and the GT is computed in two following conditions:

-Reconstruction of CTCA axial slices into cardiac standard views.

-Using Generalized Pattern Search (GPS) algorithm for Slice-to-Volume (S/V) registration [11].

MAE formulation is defined as below:

$$MAE = \frac{1}{N}\sum_{i=1}^{N}|x_i - y_i| \quad (10)$$

Where N is the number of samples of X and Y.

The validation steps are performed on A4C, A2C, PSAX, and PLAX views. Figure 5 shows CC results between the proposed method and GT. As illustrated in Figure 5, the means ($\pm$SD) of CC for A4C, A2C, PLAX, and PSAX views are 0.89 ($\pm$0.07), 0.89 ($\pm$0.07), 0.82 ($\pm$0.06), and 0.68 ($\pm$0.04), respectively. As can be inferred from the results, PSAX view has the lowest CC values. The main cause is that, since the acquired PSAX is in the mitral valve level, the field of view in this class of images is very limited. Therefore, exploring the cardiac cycle without the presence of cardiac chambers is limited. Exploring the results in different cardiac phases shows that the mean ($\pm$SD) of CC values for end-diastole, rapid-filling, end-systole, rapid-filling, reduced-filling, and atrial-contraction are 0.71($\pm$0.05), 0.84($\pm$0.1), 0.82($\pm$0.11), 0.79($\pm$0.07), 0.85 ($\pm$0.1), and 0.9 ($\pm$0.09), respectively. Figure 6 shows the evaluation results due to MAE for four standard acquisition views in six cardiac phases.

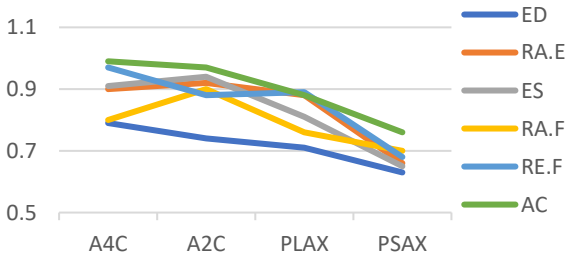

Figure 5. Computation of CC between the proposed method and the GT for six cardiac phases and four standard views

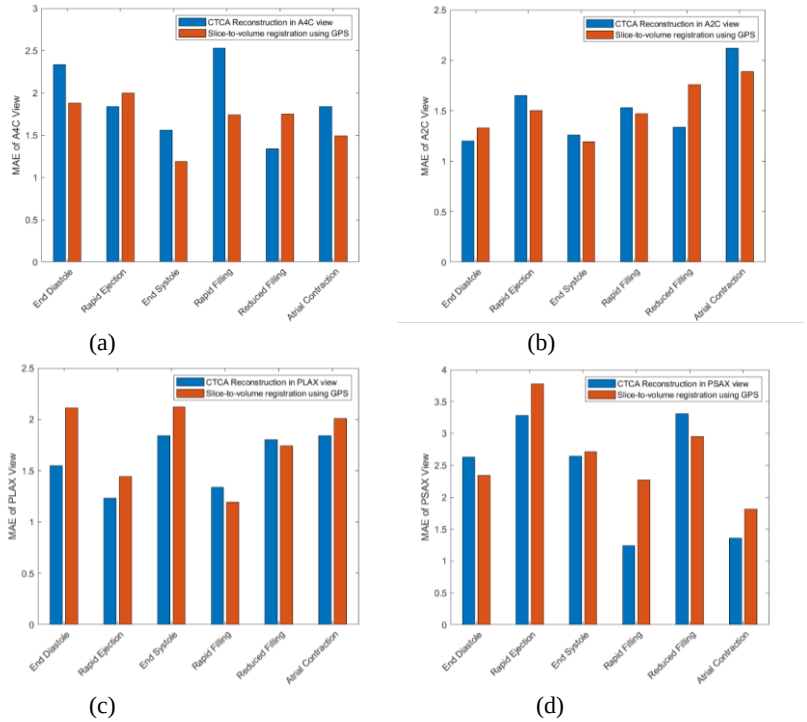

(a) (b) (c) (d)

Figure 6. MAE between frame numbers extracted from the proposed method (using two two-slice extraction methods) and from the GT for a) A4C, b) A2C, c) PLAX, and d) PSAX views

As displayed in Figure 6, using both slice extraction methods, The MAE of the resulting frame numbers from the proposed method and GT is insignificant. Hence, Figure 6 demonstrates the difference between the mean MAE of using approximate reconstruction or using GPS for the S/V registration method for six cardiac phases in four cardiac views.

As shown in Table 3, the error between the mean MAE values of two slice extraction methods in the proposed method are 0.01, 0.08, 0.16, and 0.17 for A2C, A4C, PLAX, and PSAX views, respectively. Thus, the proposed method seems robust to any spatial multimodal registration method.

Figure 7 exhibits the resulted TTE frames in four acquisition views and their corresponding percentage of RR interval in CTCA volumes for six cardiac phases. The average running time for TR of CCTA and TTE using an Intel(R) Core (TM) i7-6700HQ CPU @ 2.60 GHz, 2592 MHz, 4 Core(s), and 8 Logical Processor(s) laptop are about 2.67 ± 0.04, and 1.64 ± 0.03 seconds, respectively.

4. Discussion

An independent of user interaction and experience TR method without the need to preprocess MCIs based on the LLE algorithm is proposed. The proposed method uses only the information of images and their relations in a cardiac cycle. The LLE algorithm's main feature is maintaining local and similar points when mapping from high-dimensional to low-dimensional space.

To evaluate the proposed method, images related to CTCA and TTE modalities were recorded from ten patients who were referred to CTCA imaging by their physician. Using LLE to image sets of both modalities, the relationship among frames in high-dimensional space is well preserved, and valuable information is extracted from the manifold of images for TR between two modalities.

As it can be seen from the resulted LLE manifolds, due to the periodic nature of the cardiac cycle, the LLE manifolds of both modalities are close (for TTE) or nearly close (CTCA) curves. The reason for the expression of 'nearly close' is that CTCA data are constructed in every 10% of the RR interval. Thus, only nine cardiac phases of CTCA data are available for each patient.

By calculating the NDP of both modalities, the changes in LV volume are evident. Since the LV volume does not change significantly in isovolumetric cardiac phases, the corresponding frames in the high-dimensional space do not alter considerably. As a consequence, three minima correspond to end-diastole, end-systole, and reduced-filling cardiac phases in the NDP of both modalities. In contrast, LV volume changes significantly between each of the three aforementioned isovolumetric cardiac phases: rapid-ejection, rapid-filling, and atrial-contraction cardiac phases. Therefore, NDP contains three maxima according to these phases, and functional and anatomical features of the heart can be assessed in a cardiac cycle instead of considering only one cardiac phase in temporal registration followed by a fusion [14, 30, 31]. The mean CC of 0.81 for six cardiac phases and four acquisition views among the results of the proposed method and from frame number assignment by an expert shows the effectiveness of the proposed method. Furthermore, CC results show that, compared to the previously published articles for MCI registration, the proposed method can be used as an alternative to user-dependent ECG-labelling

Table 3. Comparison between two slice extraction methods in the proposed method

	A2C		A4C		PLAX		PSAX	
	Recon. in to standard acquisition views	**Using GPS method**	**Recon. in to standard acquisition views**	**Using GPS method**	**Recon. in to standard acquisition views**	**Using GPS method**	**Recon. in to standard acquisition views**	**Using GPS method**
End Diastole	1.20 (±0.01)	1.33 (±0.02)	2.33 (±0.01)	1.88 (±0.02)	1.55 (±0.26)	2.11 (±0.24)	2.63 (±0.35)	2.34 (±0.31)
Rapid Ejection	1.65 (±0.03)	1.50 (±0.01)	1.84 (±0.12)	2 (±0.03)	1.23 (±0.03)	1.44 (±0.06)	3.28 (±0.54)	3.78 (±0.51)
End Systole	1.26 (±0.01)	1.19 (±0.02)	1.56 (±0.06)	1.19 (±0.10)	1.84 (±0.19)	2.12 (±0.13)	2.64 (±0.62)	2.71 (±0.64)
Rapid Filling	1.53 (±0.03)	1.47 (±0.04)	2.53 (±0.24)	1.74 (±0.07)	1.34 (±0.15)	1.19 (±0.01)	1.24 (±0.52)	2.27 (±0.55)
Reduced Filling	1.34 (±0.05)	1.76 (±0.03)	1.34 (±0.12)	1.75 (±0.10)	1.80 (±0.12)	1.74 (±0.21)	3.31 (±0.42)	2.95 (±0.31)
Atrial Contraction	2.12 (±0.06)	1.89 (±0.03)	1.84 (±0.17)	1.49 (±0.06)	1.84 (±0.16)	2.01 (±0.22)	1.76 (±0.71)	1.81 (±0.63)
Mean (±SD)	**1.51 (±0.31)**	**1.52 (±0.23)**	**1.590(±0.41)**	**1.67 (±0.26)**	**1.60 (±0.24)**	**1.76 (±0.35)**	**2.47 (±0.75)**	**2.64 (±0.62)**

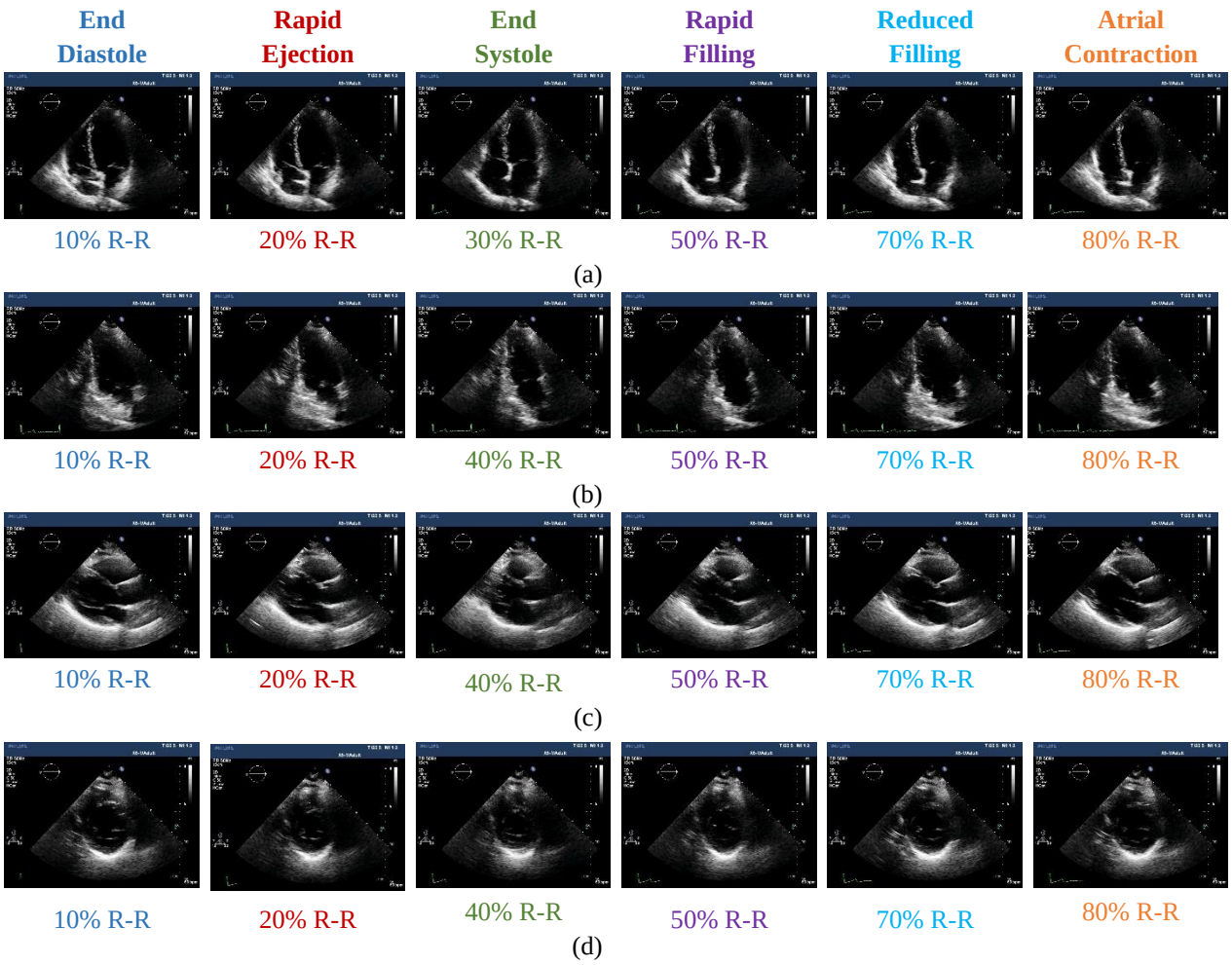

Figure 7. Resulted in TTE frames in a) A4C, b) A2C, c) PLAX and d) PSAX views. The corresponding CTCA volume due to the percentage of RR interval is stated below each frame for six cardiac phases

methods [32]. Although most echocardiography systems include ECG recording and can be assessed during diagnosis in real-time capturing or even offline analysis, in CTCA modality, ECG data are not available in offline processing. Another aspect of the ability of the proposed method versus other related works in TR is that it uses the information of the image sequence in the cardiac cycle and does not need to determine the initial condition for optimizing or pre-processing the images of both modalities to produce time series. Transcatheter aortic valve replacement and implantation are preferred minimally invasive procedures to treat aortic valve stenosis. PSAX view is used as a guide in such procedures which is a contributor to image fusion in these procedures. According to the expert's expression, accurate diagnosis of cardiac phases in the PSAX view is more difficult than other standard views. Thus, the proposed method can be a better solution for surgeon-based TR.

To investigate the robustness of the proposed method along with different spatial registration and fusion methods, the results obtained from this research are compared to using an S/V registration method [11]. The error of mean MAE between two slice extraction methods for six cardiac phases of A2C, A4C, PLAX, and PSAX views is less than 0.17. Hence, the proposed method can be used in conjunction with many spatial registration and fusion methods. PSAX view has less field of view than the other standard heart views. As a result, accessing this view is associated with more errors in both reconstruction and using GPS methods. Furthermore, the algorithm can utterly automatically synchronize MCIs. Unlike recent studies [16-18, 33], there is no need for the pre-processing of modalities in the algorithm. Consequently, it is fast, and easy to implement. Indeed, in the proposed method, since the local structure of the data is preserved when mapping from high-dimensional to low-dimensional space, it can be used in the TR of all MCIs obtained during the cardiac cycle.

5. Conclusion

A TR method of MCIs based on the LLE algorithm is presented. Compared to the major studies on TR of MCIs and based on the results and agreements to visual assessment by an expert, it can be robustly and efficiently done without using ECG signal and without any pre-processing or primary condition selection needed for both types of anatomical and functional cardiac image modalities. Besides, this study also makes it possible to consider changes in the heart and the coronary arteries compared to studies that have performed image fusion in only one cardiac phase. The proposed method can be improved by increasing the reconstructed images of CTCA in the time domain which means decreasing the distances of reconstruction points in the R-R interval to achieve dynamic synchronization of MCIs with more frames. According to the high proceeding speed of the algorithm, it can be used in real-time fusion methods in minimally invasive procedures. Also, it can be used in other cardiac modalities such as Cardiac Magnetic Resonance Imaging or 3D echocardiography.

References

1- O. World Health, World health statistics 2020: monitoring health for the SDGs, sustainable development goals. *Geneva: World Health Organization*, 2020.

2- Q. Zhang, A. Samani, and T. M. Peters, "MR and ultrasound cardiac image dynamic visualization and synchronization over Internet for distributed heart function diagnosis," *Comput Med Imaging Graph*, vol. 88, p. 101850, Mar 2021.

3- J. Jose, N. Gautam, M. Tiwari, T. Tiwari, A. Suresh, V. Sundararaj, et al., "An image quality enhancement scheme employing adolescent identity search algorithm in the NSST domain for multimodal medical image fusion," *Biomedical Signal Processing and Control*, vol. 66, p. 102480, 2021/04/01/ 2021.

4- M.-A. Azam, K.-B. Khan, M. Ahmad, and M. Mazzara, "Multimodal Medical Image Registration and Fusion for Quality Enhancement," *Computers, Materials \& Continua*, vol. 68, pp. 821-840, 2021.

5- J. Grondin, D. Wang, C. S. Grubb, N. Trayanova, and E. E. Konofagou, "4D cardiac electromechanical activation imaging," *Computers in Biology and Medicine*, vol. 113, p. 103382, 2019/10/01/ 2019.

6- T. Tada, K. Osuda, T. Nakata, I. Muranaka, M. Himeno, S. Muratsubaki, et al., "A novel approach to the selection of an appropriate pacing position for optimal cardiac resynchronization therapy using CT coronary venography and myocardial perfusion imaging: FIVE STaR method (fusion image using CT coronary venography and perfusion SPECT applied for cardiac resynchronization therapy)," *Journal of Nuclear Cardiology*, 2019/08/21 2019.

7- S. Zandieh, R. Bernt, S. Mirzaei, J. Haller, and K. Hergan, "Image fusion between 18F-FDG PET and MRI in cardiac sarcoidosis: A case series," *Journal of Nuclear Cardiology*, vol. 25, pp. 1128-1134, 2018/08/01 2018.

8- C. Nobre, M. Oliveira-Santos, L. Paiva, M. Costa, and L. Gonçalves, "Fusion imaging in interventional cardiology," *Revista Portuguesa de Cardiologia*, vol. 39, pp. 463-473, 2020/08/01/ 2020.

9- A. Peters, A. Motiwala, B. O'Neill, and P. Patil, "Novel use of fused cardiac computed tomography and transesophageal echocardiography for left atrial appendage closure," *Catheter Cardiovasc Interv*, Mar 9 2020.

10- Y. Takaya and H. Ito, "New horizon of fusion imaging using echocardiography: its progress in the diagnosis and treatment of cardiovascular disease," *Journal of Echocardiography*, vol. 18, pp. 9-15, 2020/03/01 2020.

11- A. Khalil, A. Faisal, K. W. Lai, S. C. Ng, and Y. M. Liew, "2D to 3D fusion of echocardiography and cardiac CT for TAVR and TAVI image guidance," *Med Biol Eng Comput*, vol. 55, pp. 1317-1326, Aug 2017.

12- Z. Luo, J. Cai, T. M. Peters, and L. Gu, "Intra-Operative 2-D Ultrasound and Dynamic 3-D Aortic Model Registration for Magnetic Navigation of Transcatheter Aortic Valve Implantation," *IEEE Transactions on Medical Imaging*, vol. 32, pp. 2152-2165, 2013.

13- N. Courtial, A. Simon, E. Donal, M. Lederlin, and M. Garreau, "Cardiac Cine-MRI/CT Registration for Interventions Planning," *in 2019 IEEE 16th International Symposium on Biomedical Imaging (ISBI 2019)*, 2019, pp. 776-779.

14- J. von Spiczak, R. Manka, A. Gotschy, S. Oebel, S. Kozerke, S. Hamada, et al., "Fusion of CT coronary angiography and whole-heart dynamic 3D cardiac MR perfusion: building a framework for comprehensive cardiac imaging," *Int J Cardiovasc Imaging*, vol. 34, pp. 649-660, Apr 2018.

15- B. Sturm, K. A. Powell, A. E. Stillman, and R. D. White, "Registration of 3D CT angiography and cardiac MR images in coronary artery disease patients," *The International Journal of Cardiovascular Imaging*, vol. 19, pp. 281-293, 2003/08/01 2003.

16- J. Betancur, A. Simon, B. Langella, C. Leclercq, A. Hernandez, and M. Garreau, "Synchronization and Registration of Cine Magnetic Resonance and Dynamic

Computed Tomography Images of the Heart," *IEEE J Biomed Health Inform*, vol. 20, pp. 1369-76, Sep 2016.

17- G. Kiss, A. Thorstensen, B. Amundsen, P. Claus, J. D. hooge, and H. Torp, "Fusion of 3D echocardiographic and cardiac magnetic resonance volumes," *in 2012 IEEE International Ultrasonics Symposium*, 2012, pp. 126-129.

18- F. Tavard, A. Simon, C. Leclercq, E. Donal, A. I. Hernández, and M. Garreau, "Multimodal registration and data fusion for cardiac resynchronization therapy optimization," *IEEE Trans Med Imaging*, vol. 33, pp. 1363-72, Jun 2014.

19- F. Anowar, S. Sadaoui, and B. Selim, "Conceptual and empirical comparison of dimensionality reduction algorithms (PCA, KPCA, LDA, MDS, SVD, LLE, ISOMAP, LE, ICA, t-SNE)," *Computer Science Review*, vol. 40, p. 100378, 2021/05/01/ 2021.

20- R. Pless and R. Souvenir, "A Survey of Manifold Learning for Images," *IPSJ Transactions on Computer Vision and Applications*, vol. 1, pp. 83-94, 2009.

21- A. Pournemat, P. Adibi, and J. Chanussot, "Semisupervised charting for spectral multimodal manifold learning and alignment," *Pattern Recognition*, vol. 111, p. 107645, 2021/03/01/ 2021.

22- P. Gifani, H. Behnam, A. Shalbaf, and Z. A. Sani, "Automatic detection of end-diastole and end-systole from echocardiography images using manifold learning," *Physiol Meas*, vol. 31, pp. 1091-103, Sep 2010.

23- L. P. Nijhawan, M. D. Janodia, B. S. Muddukrishna, K. M. Bhat, K. L. Bairy, N. Udupa, et al., "Informed consent: Issues and challenges," *Journal of advanced pharmaceutical technology & research*, vol. 4, pp. 134-140, 2013.

24- P. Mallia, "WASP (Write a Scientific Paper): Informed consent in research," *Early Hum Dev*, vol. 124, pp. 54-57, Sep 2018.

25- P. Orzechowski, F. Magiera, and J. H. Moore, "Benchmarking Manifold Learning Methods on a Large Collection of Datasets," *in Genetic Programming, Cham*, 2020, pp. 135-150.

26- S. T. Roweis and L. K. Saul, "Nonlinear Dimensionality Reduction by Locally Linear Embedding," *Science*, vol. 290, p. 2323, 2000.

27- L. K. Saul and S. T. Roweis, "Think globally, fit locally: unsupervised learning of low dimensional manifolds," *J. Mach. Learn. Res.*, vol. 4, pp. 119-155, 2003.

28- N. Thorstensen, "Manifold learning and applications to shape and image processing," *Ph.D., Mathematics,Computer Science*, 2009.

29- Z. Alizadeh Sani, A. Shalbaf, H. Behnam, and R. Shalbaf, "Automatic computation of left ventricular volume changes over a cardiac cycle from echocardiography images by nonlinear dimensionality reduction," *J Digit Imaging*, vol. 28, pp. 91-8, Feb 2015.

30- F. Maffessanti, K. Addetia, G. Murtagh, L. Weinert, A. R. Patel, R. M. Lang, et al., "Fusion imaging of computed tomography and 3D echocardiography: Combined assessment of coronary anatomy and myocardial function," *in Computing in Cardiology* 2014, 2014, pp. 701-704.

31- A. Khalil, Y. M. Liew, S. C. Ng, K. W. Lai, and Y. C. Hum, "Echocardiography to cardiac CT image registration: Spatial and temporal registration of the 2D planar echocardiography images with cardiac CT volume," *in 2016 IEEE 18th International Conference on e-Health Networking, Applications and Services (Healthcom)*, pp. 1-5, 2016.

32- J. J. Peoples, G. Bisleri, and R. E. Ellis, "Deformable multimodal registration for navigation in beating-heart cardiac surgery," *International Journal of Computer Assisted Radiology and Surgery*, vol. 14, pp. 955-966, 2019/06/01 2019.

33- A. Atehortúa, M. Garreau, A. Simon, E. Donal, M. Lederlin, and E. Romero, "Fusion of 3D real-time echocardiography and cine MRI using a saliency analysis," *International Journal of Computer Assisted Radiology and Surgery*, vol. 15, pp. 277-285, 2020/02/01 2020.